Is inelastic cotunneling phase coherent?*

M. Sigrist, T. Ihn, and K. Ensslin[a)]
Solid State Physics Laboratory, ETH Zurich, 8093 Zurich, Switzerland

M. Reinwald and W. Wegscheider
Institut für Experimentelle und Angewandte Physik, Universität Regensburg, Regensburg, Germany

(Received 3 August 2006; accepted 21 January 2007; published online 27 April 2007)

For low biases the linear conductance of quantum dots is based on elastic transport processes. At finite bias in the Coulomb blockade regime, inelastic cotunneling sets in once the applied bias exceeds the energy between ground and excited state in the dot. Here we report on transport experiments through an Aharonov-Bohm ring containing a quantum dot in each arm of the ring. The tunnel coupling between the two dots can be tuned by electrostatic gates. For strong tunnel coupling and low bias we observe pronounced Aharonov-Bohm oscillations in the ring with visibilities exceeding 80%. For quantum dots which are purely capacitively coupled, the Aharonov-Bohm amplitude is reduced to a more standard 10%. For finite bias, where transport through excited states becomes possible and a conductance onset is observed, the visibility of the Aharonov-Bohm oscillations remains basically unchanged, while the phase typically undergoes a change of π. We discuss these observations in view of the possible elastic and inelastic transport processes and their contributions to coherent transport. © *2007 American Institute of Physics*.
[DOI: 10.1063/1.2722725]

I. INTRODUCTION

Electron transport through quantum dots for small bias voltages can be understood based on elastic tunneling processes.[1] If the dot chemical potential is in resonance with the Fermi levels in the source and drain contacts, first-order tunneling processes dominate the conductance resonances. As the dot level is tuned off resonance, a usually small cotunneling current flows which is a process of second order.[2] For example, in this configuration the electron occupying the ground state can leave the dot toward the source contact and be simultaneously replaced by an electron from the drain contact. The overall two-electron process is energy conserving and therefore elastic. As the bias voltage across the dot is increased and exceeds the energy between the ground and first excited electronic state in the dot, the electron leaving the ground state of the dot is replaced by an electron exciting the dot to its first excited state. This process is inelastic since the dot is in an excited state after the tunneling process.[3] To check the phase coherence of these processes requires appropriate experiments. We follow the pioneering approach of Yacoby *et al.*, who embedded a quantum dot in one arm of an Aharonov-Bohm (AB) ring.[4] They found that first-order tunneling through a quantum dot at resonance contains a significant coherent contribution. This approach has been extended to the case of two quantum dots, each one embedded in one arm of the AB ring.[5,6] Here we proceed to study a highly tunable double dot-ring system, where the AB effect is used to investigate the phase coherent contributions to elastic and inelastic cotunneling currents.

II. TRANSPORT THROUGH THE OPEN RING

The sample shown in Fig. 1(a) is based on a Ga[Al]As heterostructure with a two-dimensional electron gas (2DEG) 34 nm below the surface. It was fabricated by multiple-layer local oxidation with a scanning force microscope:[7] The 2DEG is depleted below the oxide lines written on the GaAs surface [bright lines in Fig. 1(a)], thus defining the ring interferometer. A Ti film evaporated on top is cut by local oxidation [faint lines in Fig. 1(a)] into mutually isolated top gates. The quantum dots indicated by the circles in the AB loop can be tuned by in-plane gates pg1 and pg2. The tunnel coupling between the dots is controlled by the top plunger gate extended all the way across the dots. The coupling of each dot to source and drain contacts is tuned by a combination of top and in-plane gates qc/tqc 1–4. In order to characterize the ring, we open the dots completely to source and drain contacts to study the interferometer itself. For a very negative voltage applied to the top plunger gate $V_{tpg}=-150$ mV there is no current flow between the two arms of the AB ring through the center of the device. The corresponding magnetoconductance is shown with the blue curve in the bottom of Fig. 1(b). The corresponding Fourier transform plotted in blue in Fig. 1(c) shows a single peak compatible with the area of the bright orbit indicated in Fig. 1(a).

As the voltage on the top plunger gate is made more positive, the coupling between the two arms of the AB ring is

*This paper is based on a talk presented by the authors at the 28th International Conference on the Physics of Semiconductors, which was held 24–28 July 2006, in Vienna, Austria. Contributed papers for that conference may be found in "Physics of Semiconductors: 28th International Conference on the Physics of Semiconductors," AIP Conference Proceedings No. 893 (AIP, Melville, NY, 2007); see http://proceedings.aip.org/proceedings/confproceed/893.jsp

a)Electronic mail: ensslin@phys.ethz.ch

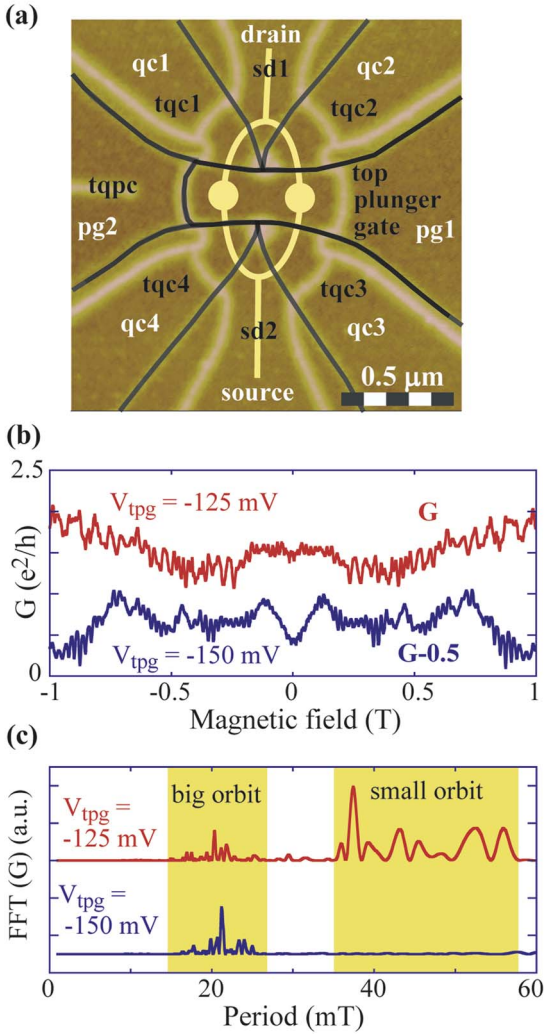

FIG. 1. (Color online) (a) SFM micrograph of the structure. In-plane gates (white letters), titanium oxide lines (black lines), and top gates (black letters) are indicated. The ring–double-dot system is illustrated by the quantum dots (full circles) and the AB loop (bright lines through QDs). (b) The conductance from source to drain through the open ring as a function of magnetic field is plotted. For the upper curve the top plunger gate was adjusted to $V_{tpg}=-125$ mV. This allows significant tunneling between the two branches of the ring. For the lower curve the coupling point contact between the branches was closed by applying a more negative voltage of $V_{tpg}=-150$ mV to the top plunger gate. AB oscillations are observed for both curves. (c) The Fourier transform as a function of period is plotted for both top plunger gate settings. An additional AB period for a small orbit is found for the case of coupled branches corresponding to interference around one oxide dot in the structure.

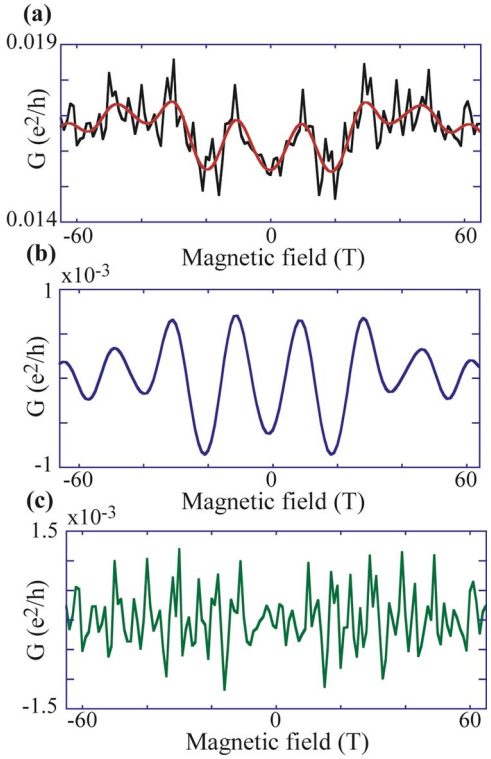

FIG. 2. (Color online) (a) A conductance trace as a function of magnetic field containing weak AB oscillations is plotted (black). The step size of the magnetic field provides about 20 data points per AB period. The superposed curve is composed of the filtered AB signal and the background conductance without the high-frequency part. (b) The filtered AB signal is plotted as a function of magnetic field. It still contains a small varying background due to the finite width of the Gauss window in Fourier space. (c) Subtracting the two curves in (a) yields the high-frequency fluctuations plotted here. Many features are symmetric in magnetic field and therefore reproducible. They mostly originate from interference effects in the contacts of the structure.

increased. The magnetoconductance resembled by the top red trace in Fig. 1(b) is taken for $V_{tpg}=-125$ mV. It clearly shows a variety of periods. The corresponding Fourier transform in Fig. 1(c) shows peaks around 20 mT periodicity, which are compatible with the large AB orbit discussed before. However, another series of peaks arises for larger periods in magnetic field being related to smaller orbit sizes. The yellow area indicates the periodicities which correspond to orbits closing along the path which connects the two quantum dots. We conclude that the size of the characteristic orbit giving rise to AB oscillations can be tuned by the top plunger gate voltage. While the present analysis was done for an open ring, it remains valid for the case where quantum dots are induced by appropriate gate voltages in the two arms of the AB ring.

III. ANALYSIS OF THE FEATURES IN MAGNETIC FIELD

The black line in Fig. 2(a) shows the magnetoconductance measured in the regime where quantum dots are induced in the two arms of the AB ring. Consequently, the average conductance is much lower than in the case of the open ring presented in Fig. 1(b). Many fine features being highly reproducible (see magnetic field symmetry) are apparent in the trace presented in Fig. 2(a). We analyze the data in the following way:[5] each magnetic field trace $G(B)$ is Fourier transformed into $F(\omega)$. This Fourier spectrum is then split according to $F(\omega)=g(\omega)F(\omega)+[1-g(\omega)]F(\omega)$ into the pure AB contribution $g(\omega)F(\omega)$ and a remaining part which contains the smoothly B-dependent background and the high-frequency components far beyond the AB frequency. The filter function $g(\omega)$ is taken from Ref. 5. In the B-domain it corresponds to taking the second derivative of $G(B)$ and convoluting it with a Gaussian of suitable width. We call the inverse Fourier transform of $g(\omega)F(\omega)$ the AB conductance. The remaining part of the spectrum $[1-g(\omega)F(\omega)]$ is further split into a low-frequency and a high-frequency part using a

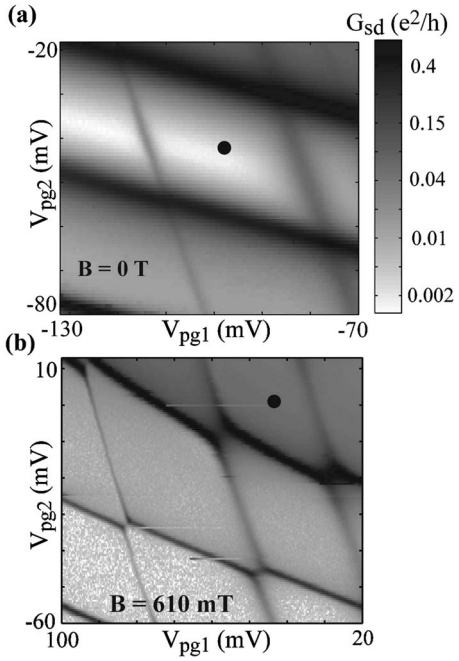

FIG. 3. (a) The charge stability diagram of double-dot system as a function of both in-plane plunger gates is shown in the regime of only capacitive coupling between the dots. The dot marks the gate settings for further finite-bias cotunneling measurements. (b) The charge stability diagram of double-dot system as a function of both in-plane plunger gates is shown in the regime of finite tunnel coupling between the dots.

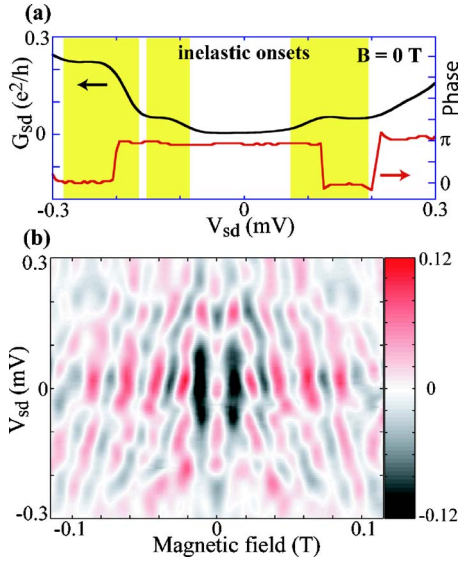

FIG. 4. (Color online) Experiments are performed for only capacitive coupling between the two dots in the cotunneling regime indicated by the black dot in Fig. 3(a). (a) In the upper curve, differential conductance is plotted as a function of DC source-drain voltage averaged over one AB period around zero magnetic field. The inelastic onsets are highlighted. The lower curve shows the phase of the AB oscillations as a function of dc source-drain bias voltage around zero magnetic field. We do not observe a phase jump for every inelastic onset. (b) The filtered AB oscillations with a period of about 22 mT are illustrated as a function of magnetic field and dc bias voltage. Slight shifts of the AB maxima as a function of bias voltage indicate a change in AB period.

low-pass type of filter function $h(\omega)$. The background conductance is then obtained as the inverse Fourier transform of $h(\omega)[1-g(\omega)]F(\omega)$.

The filtered AB signal is plotted in Fig. 2(b), the fast fluctuating background in Fig. 2(c). Throughout this analysis, we made sure that our filter procedure does not create artifacts in the AB oscillations analyzed below.

IV. TUNABLE DOUBLE DOT

The charge stability diagram of a double-dot system is typically measured as a function of gate voltages controlling the occupancy of each dot.[8,9] Figure 3 shows the conductance of the two dots embedded in the two arms of the AB ring. The two axes are the two plunger gate voltages tuning preferably the dot closer to the respective gate. Dark lines represent conductance resonances in each of the two dots. The gates also have a finite lever arm to the remote dot as indicated by the finite slope of the lines. Figure 3(a) shows the weakly coupled regime which is reached for a negative top plunger gate voltage. There is no apparent avoided crossing between resonances due to the absence of tunnel coupling and an interdot/intradot capacitance ratio of less than 1/20. As the top plunger gate is made more positive, a finite tunnel coupling and larger capacitive coupling between the dots arises, as can be seen by the gaps opening up in the charge stability diagram presented in Fig. 3(b).

V. WEAK INTERDOT COUPLING

Let us proceed by discussing the magnetic field dependence of the ring conductance in the regime where the dots are only weakly capacitively coupled [Fig. 3(a)]. The top black line in Fig. 4(a) shows the conductance versus applied bias voltage. The data are taken for a gate voltage configuration indicated by the black point in Fig. 3(a). For low biases smaller than the energy difference between ground and excited state in either of the two dots a low conductance is observed and attributed to elastic cotunneling processes. Below in Fig. 4(b) the differential conductance is plotted versus magnetic field and bias voltage. Here we present data which have been filtered according to the procedure described before. Pronounced AB oscillations are observed around zero bias voltage. As the bias voltage at $B=0$ T increased [see Fig. 4(a)], the conductance displays pronounced maxima at bias voltage of around 0.1 mV. This is taken as an indication that inelastic processes set in,[2] since the bias voltage exceeds the energy difference between the ground and excited states in one of the two dots. From Coulomb diamond measurements we can pinpoint the dot which is responsible for the inelastic onset. In the spirit of "which-path detection", we therefore know in which dot energy is dissipated if the electron relaxes from the excited state down to its ground state. The conductance map in Fig. 4(b) shows the development of the AB features as the bias voltage is increased. Overall, the visibility of the AB oscillations remains roughly constant as the "inelastic onset" is crossed in bias voltage. For large bias voltages beyond the inelastic onset the average current increases strongly and the visibility decreases as expected. If the visibility is taken as a qualitative measure for coherence, then we have no experimental indication that coherence is strongly reduced as the inelastic onset is crossed. Furthermore, we typically find phase changes of about π [see the

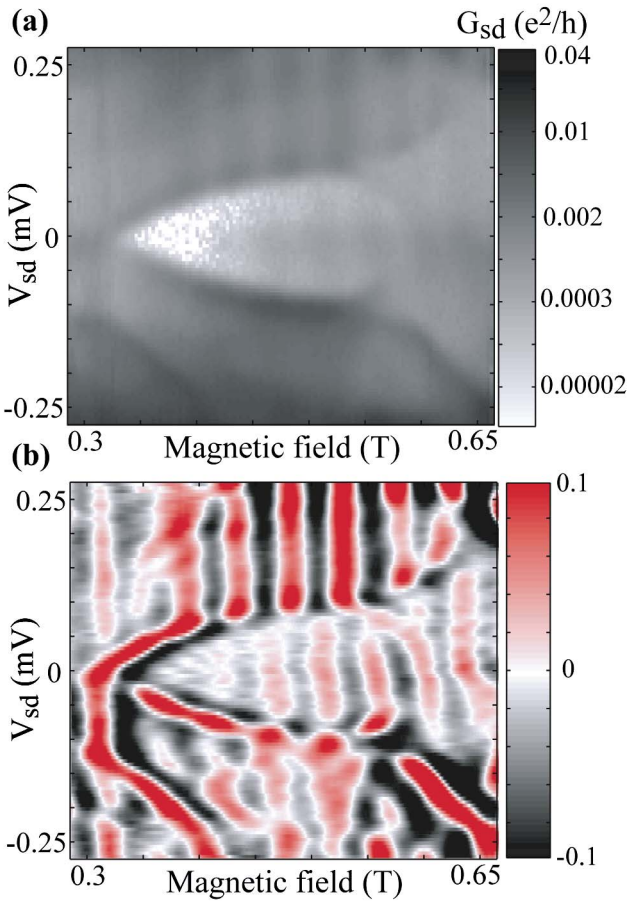

FIG. 5. (Color online) Experiments are performed for finite tunnel coupling between the two dots in the cotunneling regime indicated by the black dot in Fig. 3(b). (a) Differential conductance is plotted as a function of magnetic field and dc bias voltage on a nonlinear scale. AB oscillations with a period of about 47 mT are observed corresponding to interference around an oxide dot in the structure. (b) The normalized AB signal is illustrated as a function of magnetic field and dc bias voltage. A phase jump in the AB oscillations is observed across the inelastic onset.

bottom red trace in Fig. 4(a)] close to the bias voltages where the inelastic onsets occur. We would like to note, however, that phase changes can also occur at other bias voltages which cannot be linked to obvious excited states visible in the *I-V* characteristics across the dot. Figure 4(b) also shows that the fringes in magnetic field shift as a function of bias.

VI. STRONG INTERDOT COUPLING

Let us now turn to the case of strong interdot coupling as illustrated in Fig. 3(b). The differential conductance is plotted in Fig. 5(a) as a function of bias voltage and magnetic field. There is a clear contrast difference between the light and dark gray areas marking the onset of inelastic cotunneling. Since the magnetic field also couples to the orbital degrees of freedom, the onset is magnetic field dependent. The periodicity in magnetic field now corresponds to a smaller area, namely the orbit around one of the oxide dots. This corresponds to the open ring situation described in Fig. 1(c), where the same orbit is dominant once the coupling is increased via the top plunger gate. Using the filter routine described before, the same data are plotted in Fig. 5(b). Phase changes of π can be observed at gate voltages which can be directly related to the inelastic onsets shown in Fig. 5(a). We would like to note that the visibility of the AB oscillations can take values up to 50%–80% in this configuration.

VII. DISCUSSION

It seems surprising that a phase coherent effect can be observed in the so-called "inelastic cotunneling" regime. We can measure in which of the two dots the relevant excited state lies. Once this energy is released and the dot has relaxed back down to its ground state, in principle a which-path detection scenario has been realized, leading to a quenching of interference effects. Relaxation by phonons is thought to occur on time scales of about 10 ns.[10] In this particular case, the quantum dots are strongly coupled to source and drain and the current level in the cotunneling regime is as high as 10 pA. This corresponds to an average time between successive electrons of the order of 10 ns. It is therefore conceivable that once an inelastic cotunneling process has taken place, the next electron tunnels elastically through the excited state of the quantum dot. This transport channel is only available at bias voltages beyond the inelastic onset. Therefore, the total current flowing through the ring structure can be composed of elastic tunneling events, even in the regime where the applied bias is larger than the energy separation between excited and ground state. This is a tentative explanation for the experimental observation reported in Fig. 4, that AB oscillations persist with a significant visibility for small and large biases. The fact that the oscillations typically show a phase change of π once the excited state moves into the bias window demonstrates that most of the current indeed requires the existence of the exited state. It is important to note that the existence of a phase jump cannot always be linked to an excited state. An excited state can be there but may contribute weakly to the current because its tunnel coupling to source and drain contacts is weak. On the other hand, the current carried by different states may vary as a function of bias voltage, and therefore a phase shift can occur even if no new state becomes available in the bias window.

Once a significant tunnel coupling between the dots is realized a smaller AB orbit takes over, as discussed before. For an electron wave packet entering the ring, one part can travel through one of the dots and interfere with the part of the wave packet having taken the other path in the second dot. Interference can therefore take place in one of the dots rather than in an open part of the interferometer, as is usually the case. The dot may act as a cavity and enhance the interference, possibly giving rise to the large visibilities in this configuration. If the interference occurs in the dot where, for large biases, an excited state enters the transport window, then this process does not allow which-path detection. There are four equivalent configurations where these smaller AB orbits can play the dominant role. There can be an orbit around each of the two oxide dots shown in Fig. 1(a). Each of these orbits can be linked to the source/drain contact via either of the two remaining paths. The data in Fig. 5 link the

phase shifts observed in the AB oscillations to the onset of inelastic (and possibly elastic) cotunneling processes through the excited state.

We have investigated two different coupling regimes of the double-dot system. In both cases an excited state in one of the dots can be identified. Nevertheless, transport remains largely phase coherent. For strongly coupled dots a topologically different path becomes possible giving rise to a modified AB periodicity and therefore eliminating the possibility of a which-path detection. For weakly coupled dots, where the current path is well defined, elastic processes can occur via excited states, if the transport rates through the dot are faster than the relaxation rate of this excited state to its ground state.

VIII. CONCLUSIONS

We have presented transport experiments through a ring geometry containing a quantum dot in each arm. The tunnel coupling between the dots can be tuned by appropriate gate voltages. For increasing bias voltages, transport through an excited state in one of the dots becomes relevant. In this case the Aharonov-Bohm oscillations typically display a phase shift of π. If the tunnel coupling between the dots is switched off, the visibility of the AB oscillations remains almost unchanged when inelastic processes set in. Based on the time scales for phonon relaxation, we argue also that elastic processes can take place through the excited state which maintains phase coherence. As the tunnel coupling between the dots is turned on, a different AB orbit becomes relevant and visibilities of the AB oscillations up to 80% arise. We discuss a situation where the interference between the two paths occurs in one of the two dots, namely the one in which we have identified the inelastic onset. Therefore, which-path detection is not possible in such a configuration. Furthermore, the cavity-like situation in which the interference process takes place may explain the huge visibilities. While inelastic contributions to the cotunneling current remain incoherent in the most general situation, we have demonstrated two configurations where either a particular AB orbit or specific time constants still allow for the observation of phase coherent effects.

ACKNOWLEDGMENTS

The authors thank D. Loss, Y. Meir, and D. Sanchez for valuable discussions. Financial support from the Swiss Science Foundation (Schweizerischer Nationalfonds) is gratefully acknowledged.

[1] L. P. Kouwenhoven, C. M. Marcus, P. L. McEuen, S. Tarucha, R. M. Westervelt, and N. S. Wingreen, NATO ASI Ser., Ser. E **345**, 105 (1997).
[2] D. V. Averin and Yu. V. Nazarov, in *Single Charge Tunneling: Coulomb Blockade Phenomena in Nanostructures*, edited by H. Grabert and M. H. Devoret (Plenum Press and NATO Scientific Affairs Division, New York, 1992), p. 217.
[3] S. De Franceschi *et al.*, Phys. Rev. Lett. **86**, 878 (2001).
[4] A. Yacoby, M. Heiblum, D. Mahalu, and H. Shtrikman, Phys. Rev. Lett. **74**, 4047 (1995).
[5] M. Sigrist, A. Fuhrer, T. Ihn, K. Ensslin, S. E. Ulloa, W. Wegscheider, and M. Bichler, Phys. Rev. Lett. **93**, 066802 (2004).
[6] M. Sigrist, T. Ihn, K. Ensslin, D. Loss, M. Reinwald, and W. Wegscheider, Phys. Rev. Lett. **96**, 036804 (2006).
[7] M. Sigrist, A. Fuhrer, T. Ihn, K. Ensslin, D. D. Driscoll, and A. C. Gossard, Appl. Phys. Lett. **85**, 3558 (2004).
[8] C. Livermore *et al.*, Science **274**, 1332 (1996).
[9] W. G. van der Wiel, S. De Franceschi, J. M. Elzerman, T. Fujisawa, S. Tarucha, and L. P. Kouwenhoven, Rev. Mod. Phys. **75**, 22 (2003).
[10] T. Fujisawa, D. G. Austing, Y. Tokura, Y. Hirayama, and S. Tarucha, Nature **419**, 278 (2002).